Microsc. Microanal. 20, 1764–1771, 2014
doi:10.1017/S1431927614013506

Microscopy AND Microanalysis

Atom Column Indexing: Atomic Resolution Image Analysis Through a Matrix Representation

Xiahan Sang, Adedapo A. Oni, and James M. LeBeau*

Department of Materials Science and Engineering, North Carolina State University, Raleigh, NC 27695-7907, USA

Abstract: Here, we report the development of an approach to map atomic resolution images into a convenient matrix representation. Through the combination of two-dimensional Gaussian fitting and the projective standard deviation, atom column locations are projected onto two noncollinear reference lattice vectors that are used to assign each a unique (*i*, *j*) matrix index. By doing so, straightforward atomic resolution image analysis becomes possible. Using practical examples, we demonstrate that the matrix representation greatly simplifies categorizing atom columns to different sublattices. This enables a myriad of direct analyses, such as mapping atom column properties and correlating long-range atom column pairs. MATLAB source code can be downloaded from https://github.com/subangstrom/aci.

Key words: scanning transmission electron microscopy (STEM), projective standard deviation, atom column fitting, image analysis, atomic resolution

Introduction

Atomic resolution electron microscopy serves an essential tool to probe the local crystal structure of materials. To determine local structural or chemical relationships, analysis of these images often requires the extraction of atom column positions and intensities at the unit-cell level and beyond. For example, the incoherent imaging modes of scanning transmission electron microscopy (STEM) enable direct identification of atom column locations where the associated intensity, displacements, shape, etc., can be quantitatively retrieved. Statistical analysis of this information has enabled unit-cell level insight into material behavior through characterizing ferroelectricity (Nelson et al., 2011), composition (Robb & Craven, 2008; Van Aert et al., 2009; LeBeau et al., 2010), octahedral tilting in perovskites (Borisevich et al., 2010*a*, 2010*b*, and strain Zuo et al., 2014). Given the success of atomic resolution image analysis, but scarce discussion on the data structure used to efficiently organize hundreds of atom columns in atomic resolution images, there is a need for a broadly applicable approach that indexes the atom columns, requires only minimal user input, and is readily applicable to complex crystal structures.

Consider the case of $L1_2$ Ni_3Al viewed along <110> shown in Figure 1a. Although the atom column locations can be readily identified by normalized cross-correlation (NCC) and fitting (atom column fitting), there is often a need to differentiate sublattices, for example, Ni and Ni + Al atom columns as indicated in the figure inset. While identification can be trivial for drastically different sublattice intensities (LeBeau & Stemmer, 2008), the example in Figure 1b shows that the atom column intensity histogram for Figure 1a exhibits significant overlap between Ni + Al and Ni sites in part owing to surface contamination and/or thickness variation. As a result of this minimal site contrast, the intensity alone cannot be used to distinguish the two different sublattices despite their large intensity ratio predicted from *Z*-contrast, $28^{1.5}/((28+13)/2)^{1.5} = 1.6$.

To identify the corresponding sublattice, each atom column can be related to its neighbors through a chain-based algorithm that locates neighbors using a distance metric. In the Ni_3Al example, the four nearest neighbors can be identified by finding those the shortest distance away (if not at an edge). The sublattice type can then be inferred by the local neighbor intensities. Practically, however, this approach can be very time-consuming if there are thousands of atom columns in an image. For each atom column, the search algorithm has to iterate, and if longer range relationships are desired then additional iterations and computation become necessary.

When probing beyond the first nearest neighbors, a distance range corresponding to the n^{th} nearest neighbor can be selected. As n increases, however, the difference between the n^{th} and $(n+1)^{\text{th}}$ near neighbor distance can quickly become smaller than the experimental measurement error. Using the Ni_3Al example, the n^{th} neighbor distances are shown in Figure 1c. The first two neighbors are seemingly well separated, whereas the fourth and fifth neighbors overlap significantly. Such analysis is particularly challenging for complex crystal structures with large lattice parameters where medium to long-range distance measurements are critical.

Atomic resolution image analysis can also be complicated by surface contamination, presence of defects, or thickness variation. For example, atom columns may not be clearly resolved or may be missing from the analysis altogether. In such cases, chain-based algorithms encounter an obstacle that can require image/sample-specific programming, producing a solution that lacks generality. In light of the aforementioned

Received June 23, 2014; accepted October 9, 2014
*Corresponding author. jmlebeau@ncsu.edu

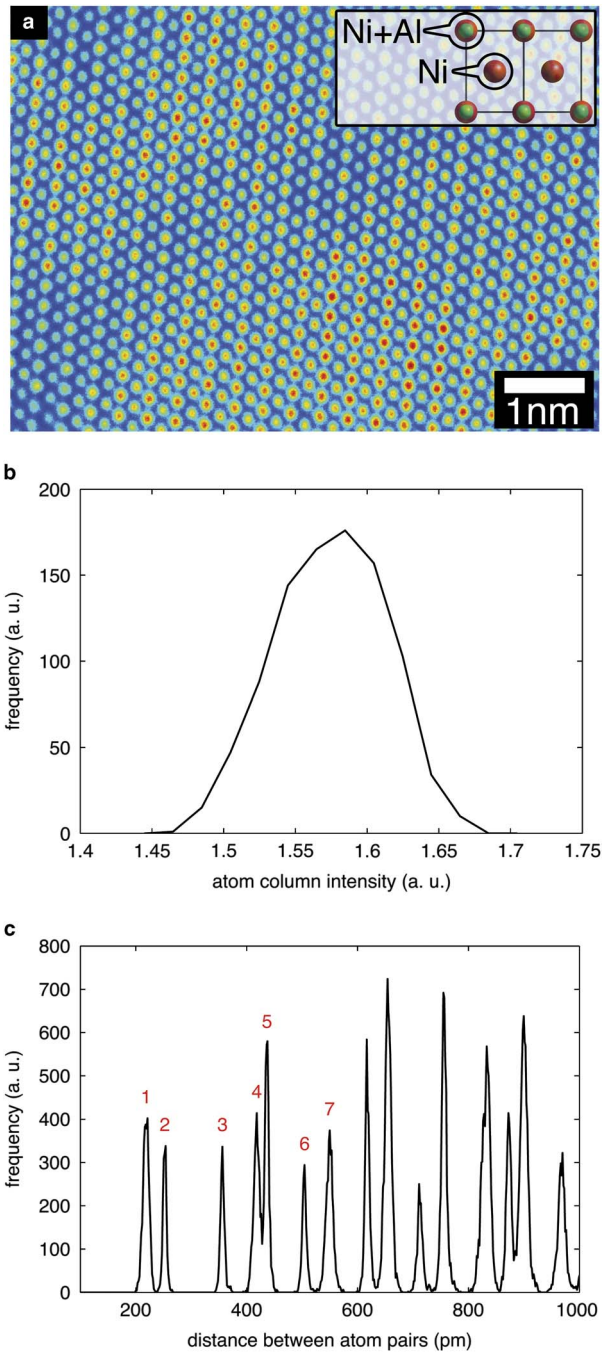

Figure 1. a: <110> Ni_3Al with significant intensity variation across the revolving scanning transmission electron microscopic image. **b:** Intensity histogram determined using the peak at each atom column location. **c:** Atom column distance histogram with a bin size of 1.6 pm. The labels indicate the first seven nearest neighbors.

issues and the recent STEM imaging developments (Jones & Nellist, 2013; Sang & LeBeau, 2014; Yankovich et al., 2014), there is a definitive need to design an efficient algorithm that can readily locate atom columns, distinguish between distinct sublattices, and relate n^{th} near neighbors.

In this article, atom column indexing is established as a methodology to transform atomic resolution images into symmetry independent matrix representations. The robust and general framework begins by combining two-dimensional (2D) atom column intensity fitting with the projective standard deviation (Sang & LeBeau, 2014). Two noncollinear lattice vectors are then selected to serve as matrix row, *i*, and column, *j*, reference directions. Each atom column is then projected onto these vectors and sorted into a unique matrix index, (i, j). After a complete description, example analyses are conducted to demonstrate atom column indexing for a variety of crystal symmetries, complexity, and defects.

Materials and Methods

As a model structure to illustrate the atom column indexing approach, $L1_2$ Ni_3Al is selected. The Ni-based super-alloy was grown using the directional Bridgman technique. As-grown crystals were annealed at 1,250°C for 14 days in He atmosphere to ensure homogeneity. Transmission electron microscopy (TEM) samples were prepared by standard twin-jet electropolishing using a solution of 10% perchloric acid in 90% methanol as the electrolyte at a temperature between − 40 and − 20°C. In addition, $\beta - Si_3N_4$ (space group $P6_3$) was examined to show that atom column indexing can be applied to symmetries without orthogonal axes. The $\beta - Si_3N_4$ sample was prepared by wedge polishing and subsequently ion-milled to electron transparency using a Fischione Model 1050 ion mill (E. A. Fischione Instruments Inc., Export, Pennsylvania, USA).

A probe-corrected FEI Titan G2 60–300 kV S/TEM (FEI, Netherlands) equipped with an extreme field emission gun source operated at 200 kV was used throughout the study. For imaging, the revolving scanning transmission electron microscopy (RevSTEM) method was applied, which uses multiple image frames acquired at different scan orientations to encode, and subsequently measure, the sample drift. After calculating the inverse transformation, the drift-induced distortion is removed from the entire image series. The frames are then registered and averaged to increase the signal-to-noise ratio. Details of the approach can be found in the study of Sang & LeBeau (2014). In this study, each frame was 1,024 × 1,024 pixels with a dwell time of 2 μs/pixel. A total of 20–40 frames were acquired with a rotation angle step size of 90°.

Framework

As atomic resolution images with 2D translational symmetry form a naturally index-able grid, the atom column positions can be represented by a matrix where two indices are used to reference each one. In this framework, the matrix row and column position, (i, j) denotes a specific atom column in the image while also maintaining neighbor connectivity. Once the atom columns are represented in this way, each index can also refer to an object containing any number of properties as shown schematically in Figure 2. For example, the image analysis may require intensity, position, shape, etc. to be investigated simultaneously. Relationships between neighbors within an image can then be readily assessed by simply

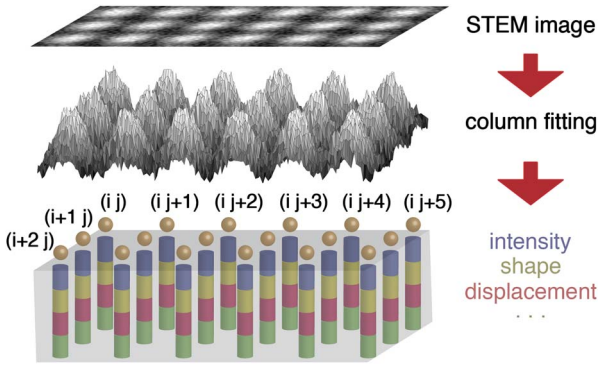

Figure 2. The atom column indexing framework begins with the experimental scanning transmission electron microscopic image (two-dimensional gray image), identifies atom column locations using Gaussian distributions (surface plot), and translates this information into a matrix where each (i, j) position can contain various properties.

examining each (i, j) position and other related columns at positions $(i+s, j+t)$. This approach enables, and greatly simplifies, a range of analysis for atomic resolution images.

Atom Column Fitting

The first step in atom column indexing requires the identification of atom column locations. As a first pass, a NCC with a Gaussian template is used to identify areas of the images that match the general atom column shape (Gonzalez & Woods, 2006; Zuo et al., 2014). Atom column locations are then identified from regions of the NCC that approach +1, whereas the background tends toward −1. Typically, the atom columns are well separated and generally contain at least ten pixels for a NCC threshold level >0.1.

Subsequently, a 2D Gaussian distribution:

$$g(x,y) = A\ \exp\left(-\frac{[(x-x_0)\cos\theta+(y-y_0)\sin\theta]^2}{\sigma_1^2}\right)\times \exp\left(-\frac{[-(x-x_0)\sin\theta+(y-y_0)\cos\theta]^2}{\sigma_2^2}\right)+Z_0, \quad (1)$$

is fit to intensities from the original image masked by the binary result of the preceding NCC threshold process. The parameters are as follows: (x_0, y_0) is the peak position, A the peak amplitude, Z_0 the background intensity, θ the rotation angle, and σ_1, σ_2 the standard deviations along the two principle axes. Note that the initial values for these parameters are critical to find the global minimum. In general, these can be estimated as follows:

(x_0, y_0)—atom column mass center defined by the NCC threshold.

Z_0—atom column median intensity minus its standard deviation.

A_0—atom column maximum intensity minus Z_0.

Using the example image in Figure 1, the 2D Gaussian fit result is shown in Figure 3a. The shape and intensity of each atom column are correctly represented by the negligible fit residual in Figure 3b. Furthermore, the relative error

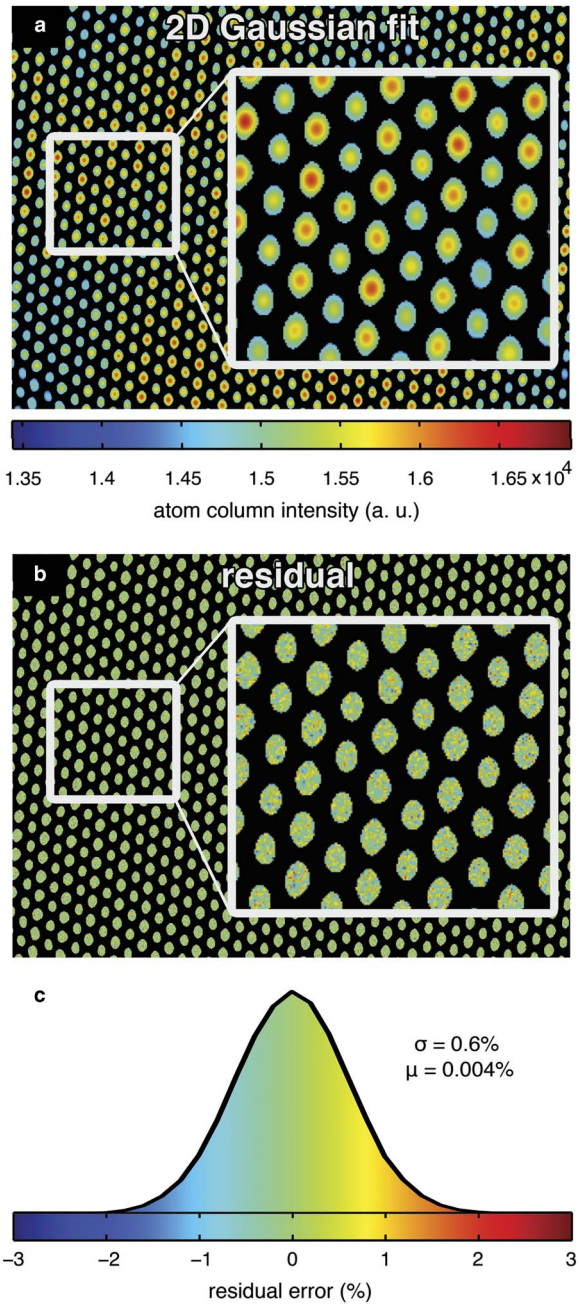

Figure 3. a: The Gaussian fit applied to the image in Figure 1a. Note the black background represents an area with normalized cross-correlation lower than the threshold and thus is not included in the fit. **b:** The residual percent error determined by the experiment and fit difference. The corresponding color scale and error histogram are shown in part (**c**).

histogram, Figure 3c, exhibits unbiased residual ($\mu = 0.004\%$) with a standard deviation of 0.6%.

Noncollinear Vector Identification

The second step in atom column indexing requires determination of any two noncollinear lattice vectors, generally low index, that define the directions for i and j.

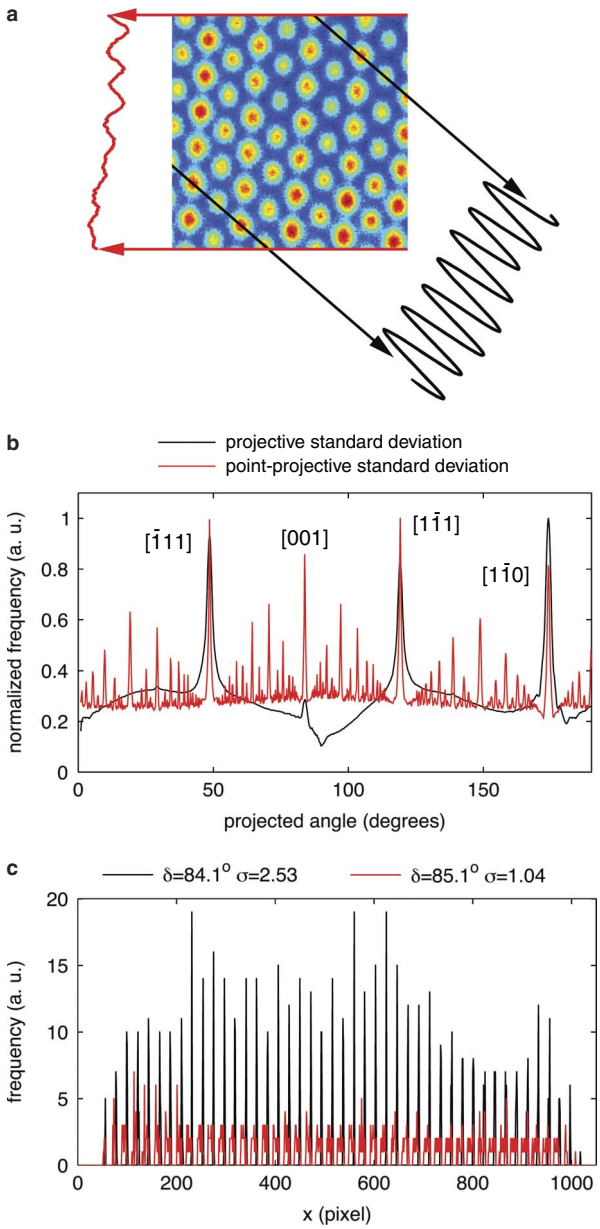

Figure 4. **a:** Projections of the experimental scanning transmission electron microscopic image along a lattice vector (black) and a random direction (red). **b:** The calculated projective standard deviation from the image intensity distribution and point-projective standard deviation from the atom column locations as a function of δ (0.2° step size). **c:** Projected line profiles for $\delta = 84.1°$ and $\delta = 85.1°$ for the image in Figure 1a.

Importantly, lattice vector identification requires accurate angle measurement to ensure that atom column positions can be readily sorted as discussed in detail below. This is achieved using the projective standard deviation method (see Sang & LeBeau, 2014 for a detailed description). At a conceptual level, the projective standard deviation begins by projecting the atomic resolution image onto a series of inclined lines (Fig. 4a), also known as the Radon transformation. When a projection is perpendicular to a lattice vector (black arrows in Fig. 4a), the normalized intensity profile maintains the periodicity of the image and exhibits a large standard deviation, σ. For projections not associated with a lattice vector, the resulting profile is flat (red arrows in Fig. 4a) and leads to a smaller σ. The projected profile σ then serves as an appropriate measure to determine lattice directions from the real-space data.

As an example, the projective standard deviation for the Ni_3Al RevSTEM image reveals the major lattice vectors given by the solid black line in Figure 4b. The [001] peak is significantly smaller owing to denser atom column packing along this direction. Using only the image intensities, the projective standard deviation can hide lattice vectors if the atom columns are too closely packed along certain directions. In the case of <110> Ni_3Al, for example, the [001] direction is not well resolved in the projective standard deviation, especially compared with [111] and [110]. To recover low-index vectors that may be obscured, the projective standard deviation analysis is then applied to the refined atom column locations. The point-projective standard deviation is defined using the atom column positions projected onto a line inclined by δ. If a projected position x falls within a pixel range, $p \leq x < p+1$, the accumulator, $A^{\delta}(p)$, is incremented by 1. For example, Figure 4c shows $A^{\delta}(p)$ along two different projection angles. For $\delta = 84.1°$, the projected profile shows well-separated peaks representing different atom column rows. For $\delta = 85.1°$,the projection direction is slightly off the lattice vector and leads to a smearing of the positions. After calculating the standard deviation, the resulting point-projective standard deviation, red line in Figure 4b, is very sensitive to small changes of the projection angle with all expected low-index vectors readily observed. When put into practice, the projective standard deviation is used to locate approximate lattice vector angles while the point-projective standard deviation is used for the final high precision angle measurement.

Defining Matrix Indices

To generate row and column indices, the atom column positions are projected onto the selected, structurally convenient lattice vectors. Figure 5a shows projections of the atom columns along [110] and [001] directions. Importantly, there is excellent separation between bins containing the atom columns, which enables each atom column to be indexed in sequence to define i from top to bottom and j from left to right. For example, atom column (17, 31) is in the 17th row from top and the 31st column from left.

The resulting matrix representation for <110> Ni_3Al shown in Figure 5b provides direct access to pure Ni sites at (odd, odd) matrix positions, while mixed Ni + Al columns are indexed at (even, even) matrix positions. This provides convenient access to calculate distances or to probe atom column intensities. As an example, the nearest neighboring atom columns for any atom column (i, j) are given at indices $(i-1, j-1)$, $(i-1, j+1)$, $(i+1, j-1)$, and

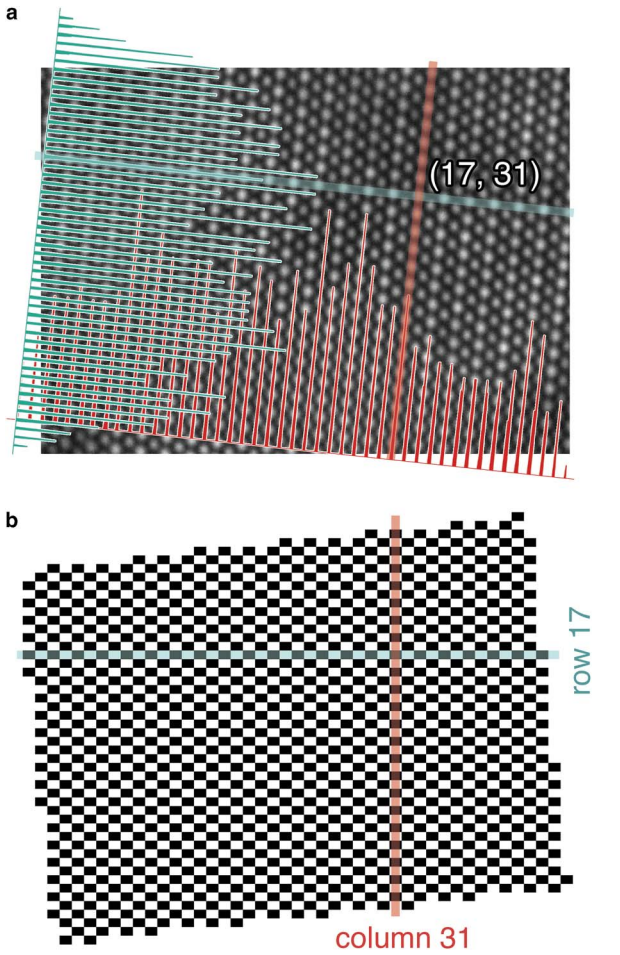

Figure 5. **a**: Projected line profiles perpendicular to the two nonlinear lattice vectors determined from point-projective standard deviation: [110] (red) and [001] (green). **b:** The corresponding matrix representation for (**a**) with black squares representing atom columns and white representing null positions. The atom column located at the 17th row and 31st column is indicated in both (**a**) and (**b**).

$(i+1,\ j+1)$.Within this indexing scheme, there are also matrix positions that do not correspond to atom column locations, for example (16, 31). At these positions, a null object is assigned. This is critical as the matrix then maintains neighbor connectivity across all indices in a consistent manner. In this way, the matrix representation is particularly useful for calculating or mapping atom column properties across an image.

Applications

Atom Column Property Mapping

Atom column intensities, distances, or local strains are all essential parameters that have been used to answer a wide range of materials science questions using the electron microscope. While a complete listing or demonstration of possible analyses is beyond the scope here, consider the

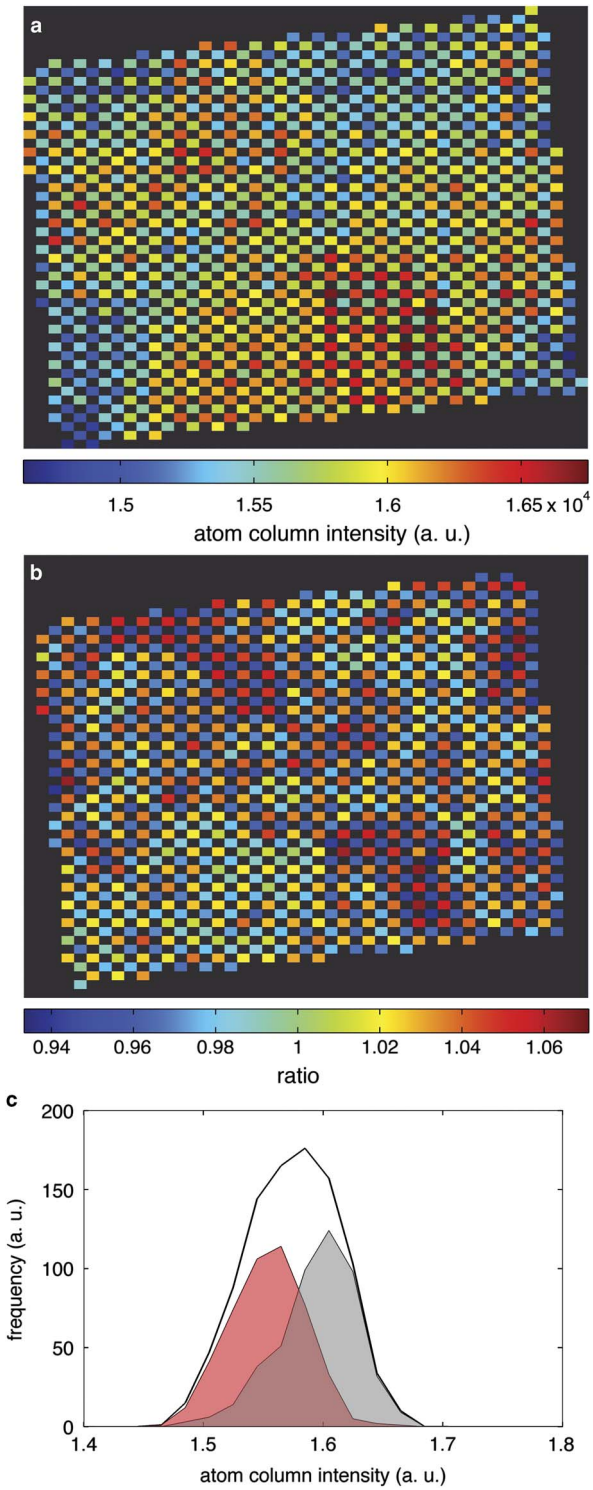

Figure 6. Atom column intensity (**a**) and ratio (**b**) maps determined from the Ni_3Al revolving scanning transmission electron microscopic image in Figure 1a. **c:** Decomposed intensity histogram calculated from Ni (red area) and Ni + Al (gray area) sublattices. The total histogram is given by the thick black line.

Ni_3Al test case where a chemical ordering map is needed. As shown in Figure 6a, the Ni_3Al atom column intensities exhibit variation that obscures ordering. To limit the

influence of this variation, the intensity ratio, R_{ij}, for an atom column at (i, j) can be determined using the equation:

$$R_{ij} = 4I(i,j)\left[\sum_{s,t=\pm 1} I(i+s, j+t)\right]^{-1}, \qquad (2)$$

where the summation is over the four nearest neighbor indexes. The resulting ratios, Figure 6b, reveal the ordered structure where the Ni positions are consistently larger than the mixed Ni + Al sites. Note that the I_{Ni}/I_{Ni+Al} ratio (1.05) is much less than the theoretical ratio predicted from Z-contrast, $28^{1.5}/((28+13)/2)^{1.5} = 1.6$, because the background intensity is included in the calculation (Klenov & Stemmer, 2006). With the matrix representation in hand, the intensity histogram presented in Figure 1b can be decomposed into the distinct Ni + Al or Ni sublattice contributions as provided in Figure 6c. Through direct real-space analysis enabled by the matrix representation, the structural and chemical details can then be analyzed to identify other features and defects, such as anti-phase boundaries.

The atom column indexing method also enables convenient enumeration of all n^{th} nearest neighbors in the image. For example, this information is useful to determine the relative displacements in ferroelectric perovskites (Nelson et al., 2011). Using the matrix representation, distance can be easily calculated by using the position information stored with each atom column object. Each n^{th} nearest neighbor can then be found to separate the distance histogram in Figure 1c. The first seven nearest neighbors are shown in Figure 7 (different colors) and superimposed on the original histogram. As highlighted in the inset, even the first and second like neighbor distances actually overlap for a few atom column positions.

While a chain-based algorithm would require additional tests, atom column indexing accomplishes accurate separation without additional overhead. Moreover, with all orders of nearest neighbors enumerated, correlation of atom column properties, such as size, shape, intensity, etc., can be readily determined on a sublattice-specific basis.

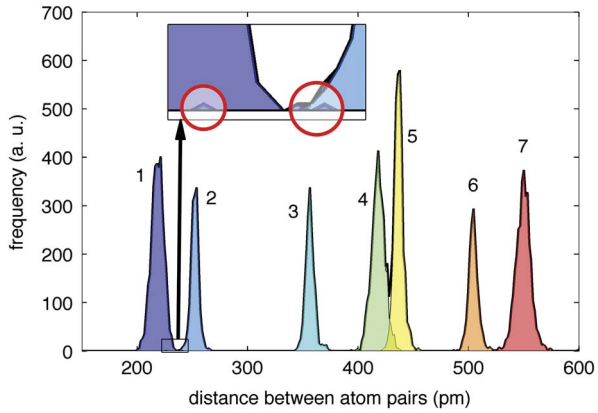

Figure 7. Distance histogram calculated from the first seven nearest neighbors using the matrix index approach. Each colored area represents atom pairs with fixed matrix separation, where the number denotes n^{th} near neighbors. The enlarged inset shows overlap between the seemingly well-separated first and second near neighbors.

Defect and Interface Analysis

While defects and interfaces typically pose an image analysis challenge, the atom column indexing method can handle a variety of cases where symmetry is related across a boundary, for example, twin boundaries or epitaxial films. Consider, for example, the {111} Ni_3Al twin boundary shown in Figure 8a. To form a matrix representation, atom column indexing is performed separately on both sides of the twin. The left and the right part have the same <111> lattice vector but different <110> as also indicated in the figure.

The projected point-projective standard deviation profile along the common <111> shows well-separated peaks that are used to determine j for each atom column, as in Figure 8b. Note that the twin boundary is located at $j = 13$.

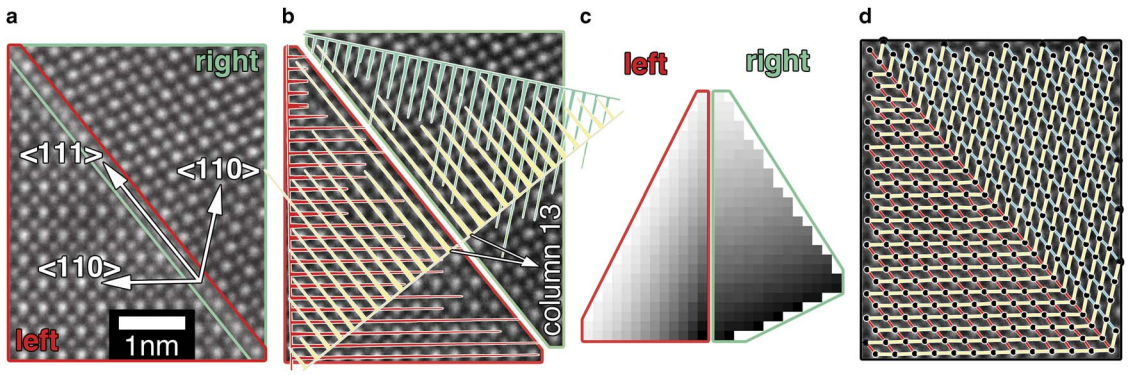

Figure 8. **a**: Ni_3Al {111} twin boundary where the image can be divided into left (red box) and right (green box) portions. **b:** Projected line profile from the left and right parts along the common <111> lattice vector (yellow) and different <110> lattice vectors (red and green). **c:** The separate matrix representations from the left and right portions. **d**: Lines connect adjacent positions in the matrix representation where each row index is connected by yellow lines. The red and green lines connect the columns from the the left and right portions, respectively.

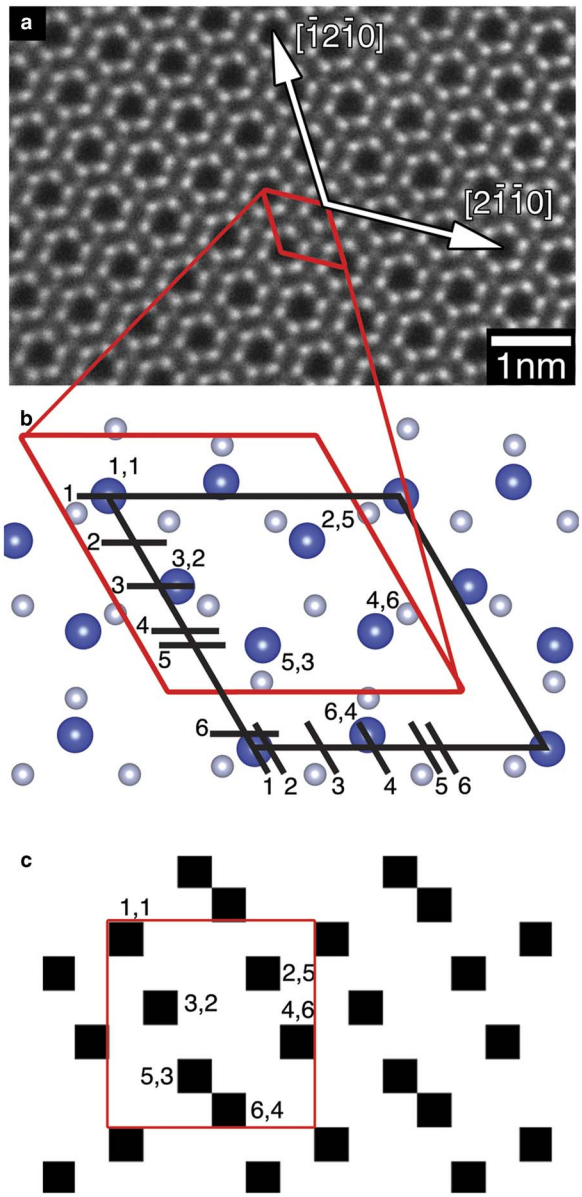

Figure 9. a: <0001> $\beta-Si_3N_4$ revolving scanning transmission electron microscopy image and (**b**) corresponding projected crystal structure where the black lines and ticks indicate atom column's rows and columns. (**c**) Matrix presentation of the same unit-cell area. The atoms are indexed in both (**b**) and (**c**). In each case, the red box indicates the repeating unit cell.

For those atom columns in the left half, that is $j \leq 13$, i is assigned by projecting along the corresponding <110>. Similarly, the right half of atom columns are those with $j \geq 13$ and i defined by projecting along the right side <110>. The resulting matrix representations are shown in Figure 8c. The two matrices are then concatenated along their mid-section where the i index is identical for both halves of the twin (Fig. 8d).

When symmetry is completely broken, for example, at a grain boundary or heterointer face, atom column indexing is unable to create a consistent matrix representation for the entire image. This challenge is universal to other analysis approaches such as geometrical phase analysis or template matching (Hÿtch et al., 1998; Zuo et al., 2014). Rather than attempt to place all atoms within the same matrix, the image can be sectioned by the user at an interface, and analyzed separately. Even if the selected areas are limited in size (pixels), the projective standard deviation can still be readily used to determine lattice vectors (Sang & LeBeau, 2014). In this way, complications owing to symmetry mismatch in an image can be avoided.

Complex Structure Analysis

While atom column indexing is straightforward for Ni_3Al, the method is readily applicable to more complex structures and symmetries. As an example, a high-angle annular dark-field STEM image of $\beta-Si_3N_4$ viewed along <0001> is presented in Figure 9a. Each projected unit cell contains six Si and eight N atom columns as indicated by the red unit cell. Applying atom column indexing, the projected crystal structure and corresponding matrix representation are shown in Figures 9b and 9c. The Si atom columns have been indexed with respect to two <11$\bar{2}$0> vectors, noting that the selected vectors are not perpendicular. All Si atom columns are readily mapped into the matrix representation across the entire image, even though the separation between rows 4 and 5 is only 36.2 pm.

Further inspection of Figures 9b and 9c reveals that the matrix representation does not resemble the projected six-fold symmetry of <0001>. Even so, the neighbor connectivity is maintained when the rows and columns are connected back to the projected structure. Namely, the complete unit cell repeats every sixth row or column. This can be seen by beginning at the top left of the unit cell and indexing each atom column as labelled in the single unit cell of Figure 9b. For an atom column (i, j), the six nearest atom columns with the same chemical environment can be readily listed as $(i+6, j)$, $(i-6, j)$, $(i, j+6)$, $(i, j-6)$, $(i+6, j-6)$, and $(i-6, j+6)$. Once the atom column—matrix relationships are identified, image analysis can proceed directly.

Conclusions

The atom column indexing framework enables the capability to map atomic resolution images into a matrix. The major advantage of the resulting representation lies in the ability to easily and universally access short-, medium-, and long-range atom column positions on a site-specific basis. Furthermore, atom column indexing works seamlessly across interface between materials with similar crystal structures, twins, anti-phase boundaries, etc. as long as there are at least two noncollinear lattice vectors in common. By storing each atom column object with a variety of properties, unprecedented flexibility in quantitative analyses becomes possible. In this way, complex analysis operations, such as calculating n^{th} nearest neighbor distances, become almost trivial tasks.

Acknowledgments

The authors acknowledge support from the Air Force Office of Scientific Research (Grant No. FA9550-12-1-0456) and the Analytical Instrumentation Facility (AIF) at North Carolina State University, which is supported by the State of North Carolina and the National Science Foundation. The authors also acknowledge Erica Corral at the University of Arizona for providing the sample of $\beta - Si_3N_4$.

References

Borisevich, A.Y., Chang, H.J., Huijben, M., Oxley, M.P., Okamoto, S., Niranjan, M.K., Burton, J.D., Tsymbal, E.Y., Chu, Y.H., Yu, P., Ramesh, R., Kalinin, S.V. & Pennycook, S.J. (2010*a*). Suppression of octahedral tilts and associated changes in electronic properties at epitaxial oxide heterostructure interfaces. *Phys Rev Lett* **105**, 087204.

Borisevich, A.Y., Ovchinnikov, O.S., Chang, H.J., Oxley, M.P., Yu, P., Seidel, J., Eliseev, E.A., Morozovska, A.N., Ramesh, R., Pennycook, S.J. & Kalinin, S.V. (2010*b*). Mapping octahedral tilts and polarization across a domain wall in $BiFeO_3$ from Z-contrast scanning transmission electron microscopy image atomic column shape analysis. *ACS Nano* **4**(10), 6071–6079.

Gonzalez, R.C. & Woods, R.E. (2006). *Digital Image Processing*, 3rd ed. Upper Saddle River, NJ, USA: Prentice-Hall Inc.

Hÿtch, M.J., Snoeck, E. & Kilaas, R. (1998). Quantitative measurement of displacement and strain fields from HREM micrographs. *Ultramicroscopy* **74**(3), 131–146.

Jones, L. & Nellist, P.D. (2013). Identifying and correcting scan noise and drift in the scanning transmission electron microscope. *Microsc Microanal* **19**(04), 1050–1060.

Klenov, D.O. & Stemmer, S. (2006). Contributions to the contrast in experimental high-angle annular dark-field images. *Ultramicroscopy* **106**(10), 889–901.

LeBeau, J.M., Findlay, S.D., Allen, L.J. & Stemmer, S. (2010). Standardless atom counting in scanning transmission electron microscopy. *Nano Lett* **10**(11), 4405–4408.

LeBeau, J.M. & Stemmer, S. (2008). Experimental quantification of annular dark-field images in scanning transmission electron microscopy. *Ultramicroscopy* **108**(12), 1653–1658.

Nelson, C.T., Winchester, B., Zhang, Y., Kim, S.-J., Melville, A., Adamo, C., Folkman, C.M., Baek, S.-H., Eom, C.-B., Schlom, D.G., Chen, L.-Q. & Pan, X. (2011). Spontaneous vortex nanodomain arrays at ferroelectric heterointerfaces. *Nano Lett* **11**(2), 828–834.

Robb, P.D. & Craven, A.J. (2008). Column ratio mapping: A processing technique for atomic resolution high-angle annular dark-field (HAADF) images. *Ultramicroscopy* **109**(1), 61–69.

Sang, X. & LeBeau, J.M. (2014). Revolving scanning transmission electron microscopy: Correcting sample drift distortion without prior knowledge. *Ultramicroscopy* **138**, 28–35.

Van Aert, S., Verbeeck, J., Erni, R., Bals, S., Luysberg, M., Van Dyck, D. & Van Tendeloo, G. (2009). Quantitative atomic resolution mapping using high-angle annular dark field scanning transmission electron microscopy. *Ultramicroscopy* **109**(10), 1236–1244.

Yankovich, A.B., Berkels, B., Dahmen, W., Binev, P., Sanchez, S.I., Bradley, S.A., Li, A., Szlufarska, I. & Voyles, P.M. (2014). Picometre-precision analysis of scanning transmission electron microscopy images of platinum nanocatalysts. *Nat Commun* **5**, 4155.

Zuo, J.-M., Shah, A.B., Kim, H., Meng, Y., Gao, W. & Rouviere, J.-L. (2014). Lattice and strain analysis of atomic resolution Z-contrast images based on template matching. *Ultramicroscopy* **136**, 50–60.